RESEARCH ARTICLE

Biomechanics of Turtle Shells: How Whole Shells Fail in Compression

PAUL M. MAGWENE[1] AND JOHN J. SOCHA[2]*
[1]Committee on Evolutionary Biology, University of Chicago, Chicago, Illinois
[2]Department of Organismal Biology and Anatomy, University of Chicago, Chicago, Illinois

JOURNAL OF EXPERIMENTAL ZOOLOGY PART A ECOLOGICAL GENETICS AND PHYSIOLOGY
A Journal of Integrative Biology

ABSTRACT

Turtle shells are a form of armor that provides varying degrees of protection against predation. Although this function of the shell as armor is widely appreciated, the mechanical limits of protection and the modes of failure when subjected to breaking stresses have not been well explored. We studied the mechanical properties of whole shells and of isolated bony tissues and sutures in four species of turtles (*Trachemys scripta*, *Malaclemys terrapin*, *Chrysemys picta*, and *Terrapene carolina*) using a combination of structural and mechanical tests. Structural properties were evaluated by subjecting whole shells to compressive and point loads in order to quantify maximum load, work to failure, and relative shell deformations. The mechanical properties of bone and sutures from the plastral region of the shell were evaluated using three-point bending experiments. Analysis of whole shell structural properties suggests that small shells undergo relatively greater deformations before failure than do large shells and similar amounts of energy are required to induce failure under both point and compressive loads. Location of failures occurred far more often at sulci than at sutures (representing the margins of the epidermal scutes and the underlying bones, respectively), suggesting that the small grooves in the bone created by the sulci introduce zones of weakness in the shell. Values for bending strength, ultimate bending strain, Young's modulus, and energy absorption, calculated from the three-point bending data, indicate that sutures are relatively weaker than the surrounding bone, but are able to absorb similar amounts of energy due to higher ultimate strain values. *J. Exp. Zool. 319A:86–98, 2013.* © 2012 Wiley Periodicals, Inc.

J. Exp. Zool. 319A:86–98, 2013

How to cite this article: Magwene PM, Socha JJ. 2013. Biomechanics of turtle shells: How whole shells fail in compression. J. Exp. Zool. 319A:86–98.

The turtle shell serves an obvious function—protection. The defensive value of a well-ossified system of plates surrounding soft tissues is easily appreciated, but the shell also plays a structural role in other behaviors such as in force production during locomotion and ventilatory movements during breathing (Landberg et al., 2003). Furthermore, it also provides non-structural functions including lactate sequestration (Jackson, '97) and vibration and tactile perception (Rosenberg, '86). The turtle shell is thus a multi-functional system, with characteristics that likely reflect the product of multiple selective pressures and trade-offs. Understanding the structural role of the shell in defense therefore requires detailed investigation.

The turtle shell is constructed of two major parts—the dorsal carapace and the ventral plastron (Fig. 1), which are connected laterally by a region known as the bridge. This box-like structure is formed of plate-like bones covered by epidermal scutes, which are keratinous and flexible. At hatching, the carapace is no more than a covering of scutes over weakly ossified ribs and connective tissue (Zangerl, '69). The plastral elements are slightly more developed (Rieppel, '93), but also afford little protection; the plates are relatively thin and have large fontanelles (i.e., unossified

Paul M. Magwene and John J. Socha contributed equally to this work.
The present address of Paul M. Magwene is Department of Biology, Duke University, Durham, NC.
The present address of John J. Socha is Department of Engineering Science and Mechanics, Virginia Tech, Blacksburg, VA 24061.
*Correspondence to: John J. Socha, Department of Engineering Science and Mechanics, Virginia Tech, Blacksburg, VA 24061.
E-mail: jjsocha@vt.edu
Received 13 March 2012; Revised 1 October 2012; Accepted 8 October 2012
Published online 30 November 2012 in Wiley Online Library (wileyonlinelibrary.com).
DOI: 10.1002/jez.1773

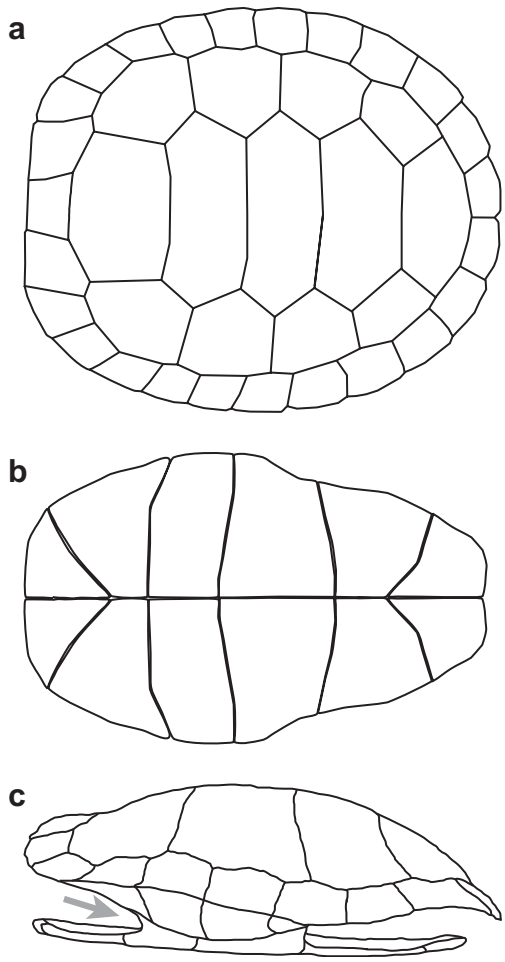

Figure 1. Emydid turtle shell morphology, showing epidermal scutes. (a) Carapace, shown in dorsal view. (b) Plastron, shown in ventral view. (c) Carapace (top) and plastron (bottom) connected by the bridge (arrow), shown in side view. Anterior is to the left.

spaces) between them. At this point, it is likely that the shell offers only slight defensive value, as evidenced by the wide variety of animals that prey on hatchling turtles. As growth proceeds, the bone thickens and the dermal plates ossify, which must increase the mechanical integrity of the shell, but ontogenetic effects on shell properties have not been studied. Mortality among young animals is relatively high, and survivorship rates are in the range of 0.18–0.35 (Congdon and Gibbons, '90; Iverson, '91). Estimates of annual survivorship for adults are much higher, in the range 0.76–0.98 (Congdon and Gibbons, '90), suggesting that the fully developed shell is a much more effective mechanical structure for defense.

The most extreme mechanical forces that a turtle shell must endure likely result from predatory attacks, reports of which are largely anecdotal (however, see Heithaus et al., 2008). Predators known to inflict damage to the shells of subadult and adult individuals of freshwater and terrestrial species include mammals (Ernst et al., '94), birds (Branch and Els, '90; Ernst et al., '94), reptiles (Ernst et al., '94), and invertebrates (Franklin, 2007). There are also reports of interspecific attacks resulting in severe shell damage or death (Shipman et al., '94). Small to medium sized predators may gnaw at the margins of the shell, whereas larger predators such as adult alligators probably apply localized forces using a row of blunted teeth (Erickson et al., 2003). Jaguars are known to use their broad-tipped canines to break the carapace of adult turtles, and enlarge the hole until the body can be removed (Emmons, '89). Avian predators may drop turtles from great heights in order to induce shell fracture (Branch and Els, '90; Walley, '93), or may use their bills to peck at the shell. Overall, the types of loading on the turtle shell can be characterized as compressive loads (from broad to point), low frequency fatigue loads, or in the case of dropping, impact loads.

Despite, or perhaps as a result of, the obvious functional role of the turtle shell in defense, historically little research has been done to assess the efficacy of the shell for bearing mechanical loads. Richmond ('64) suggested that in addition to serving as ventral armor, the plastron might function mechanically to brace the carapace as a tensile element. Bramble and coauthors (Bramble, '74; Bramble et al., '84) suggested that, though plastral kinesis in emydid and kinosternid turtles increases protection, the ventral hinge that enables the anterior shell to close may mechanically weaken the plastron. Ramaekers ('79) discussed the rheological behavior (in particular, dynamic shear modulus and damping) of shell bone from one turtle species. However, none of these studies addressed questions related to the failure properties of the shell as a whole.

Recently, there has been a renewed interest in understanding how the turtle shell functions as a mechanical system, with studies taking two general approaches. The first approach has been to analyze the components of the shell, using bending and compression tests, nano- and micro-indentation, and modeling to determine the mechanical properties of the individual elements that comprise the shell system (Krauss et al., 2009; Rhee et al., 2009; Balani et al., 2011; Damiens et al., 2012). This work has provided a baseline knowledge of the mechanical behavior of turtle shell tissues, including the first rigorous measurements of characteristics such as stiffness and hardness. The second approach has been to consider the turtle shell as a whole, using mathematical modeling (finite element analysis, FEA) to simulate the stresses that are created under different compressive loading regimes, in some cases complimented by compression tests of real shells (Stayton, 2009, 2011; Rivera and Stayton, 2011; Vega and Stayton, 2011; Zhang et al., 2012a,b). Some of these studies have linked the structural design of the shell to ecologically relevant variables; for example, relatively flat and streamlined shells that are well-suited for aquatic swimming pay a price in performance

by being less resistant to predatory loading, and females may have stronger shells than males. Overall, these studies aim to understand the mechanical implications of shell shape and morphology.

In this study we ask, How do turtle shells fail under the types of compressive loading regimes that may occur during a predatory attack? Previous whole-shell studies have examined compressive loading primarily through finite element modeling, which is proving to be a powerful technique for discovering broad principles of design in turtles. However, such mathematical models often require simplifying assumptions (e.g., uniformity of material properties) and therefore are most useful for comparative analyses. The shell is better understood as a composite system with interlocking elements (Krauss et al., 2009), with complexity in the bone, sutures, and keratin scutes across the micro- to macro-scales (Balani et al., 2011). Such complexity suggests that analyses of failure are most accurately conducted using real specimens, but many of the previous experimental studies have analyzed single specimens or even used dried shells, which cannot capture the range of variation inherent in biological systems. Furthermore, all recent theoretical and experimental studies of turtle shells have neglected the internal soft tissues within the body, and this anatomy may further complicate patterns of stress and strain in the real turtle shell when loaded. Therefore, we examined how turtle shells fail using whole animals with intact, hydrated tissues included. Because the loading involved in the various types of attack that are encountered by turtles in the wild has not been determined, we used two regimes of compressive loading, broad and pointed, to simulate the extremes of a biting attack. From the perspective of whole shells, this study addresses issues that include the strength of shells and modes of failure. Additionally, we compare the mechanical properties of sutures and bony tissues and analyze mineral content to provide a first-order characterization at a finer level of biological organization. Overall, this study adds to our growing understanding of the mechanical characteristics of the turtle shell and its role as a multi-functional structure whose properties may change with size and age.

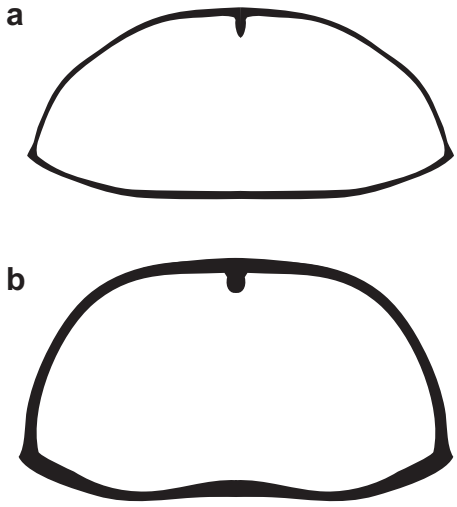

Figure 2. Cross-sections through the shell of (a) *Trachemys scripta* and (b) *Terrapene carolina* specimens, illustrating differences in external shell morphology between low-domed and high-domed taxa.

MATERIALS AND METHODS

Animal Collection and Care

To explore variation among turtles, we examined four species: *Trachemys scripta elegans* (red-eared slider), *Malaclemys terrapin* (diamondback terrapin), *Chrysemys picta* (painted turtle), and *Terrapene carolina* (box turtle). All four species are members of the family Emydidae (Ernst et al., '94), with *Trachemys*, *Chrysemys*, and *Malaclemys* more closely related as members of the clade Dierochelyinae (Gaffney and Meylan, '88; Seidel and Atkins, '89). *Trachemys* and *Chrysemys* occupy freshwater habitats, whereas *Malaclemys* lives in estuarine environments (Ernst et al., '94). The box turtles, *Terrapene*, are terrestrial in habitat. The carapaces of the three semi-aquatic taxa form relatively wide, low domes (Fig. 2a). Box turtles, on the other hand, have a high domed carapace (Fig. 2b) and possess a modified hyo-hypoplastral suture that forms a movable hinge (Fig. 3b) and allows the animal to completely enclose the head and limbs inside the shell.

Individuals of each species were either wild collected (*Terrapene*, *Chrysemys*, *Trachemys*; Illinois DNR Scientific Permit No. NH98.0385), laboratory hatched and raised (*Malaclemys*), or obtained from a commercial dealer (*Trachemys*). The exact ages of specimens were unknown except for those of *Malaclemys*, which were sub-adult. Animals were maintained under institutionally approved laboratory conditions for a period of up to six months (University of Chicago Animal Care and Use Protocol Committee protocol #70668). Animals were fed three times per week with a diet that included commercial turtle food supplemented with calcium, fish chunks, and lettuce and fruits in the case of the box turtles. All individuals were kept on a 12-hr light cycle, using full spectrum fluorescent bulbs to promote normal skeletal growth. The *Terrapene* and *Malaclemys* specimens were also used as part of a skeletal growth study and received three injections (20 mg/kg) of the fluorescent dye calcein at 1-month intervals over the course of their laboratory maintenance. It is assumed that these low doses of calcein did not affect shell mechanical properties. All animals were euthanized with intramuscular injections of sodium pentobarbitol, and then frozen at −20°C for up to 8 months. Prior to the loading experiments, specimens were allowed to thaw slowly at room temperature or in lukewarm water. We froze specimens so that all testing could occur at the same time. Although fresh tissue is ideal, previous work has indicated that one cycle of freezing has

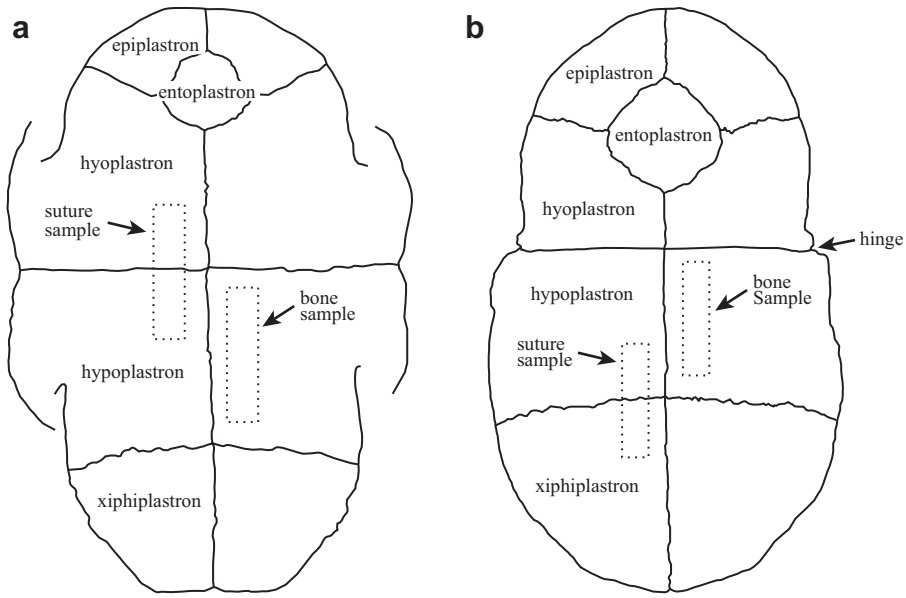

Figure 3. Locations of tissue samples used to quantify mechanical properties of bone and suture. (a) *Trachemys scripta* and *Chrysemys picta* specimens; (b) *Terrapene carolina* specimens. The hinge refers to the transverse suture that enables plastral kinesis.

little affect on material properties of mammalian bone tissue (Pelker et al., '83; Borchers et al., '95; Moreno and Forriol, 2002). To best simulate loads on the shell that may occur in a natural condition, the whole-body specimens were not altered in any way prior to testing, including removal of scutes or internal soft tissues.

Whole Shell Loading

A series of quasi-static loading experiments were conducted on the euthanized whole specimens using both broad and point compressive loading, spanning the range from a diffuse compression to a pointed penetration (such as a tooth). The broad compression loading also provides a first-order mechanical characterization of turtle shells. The goals of these experiments were to determine maximum loads, work to failure, and the location and type of fractures that occur at failure. Compressive loading experiments were conducted with specimens of all four species (10 *T. scripta* specimens, 3 specimens for each of the other species); only *T. scripta* individuals were used in the point loading experiments (7 specimens).

Specimens were loaded to failure using a tensometer (Monsanto Co., St. Louis, MO) with a custom-made loading apparatus consisting of two steel plates (plate thickness, 15.7 mm; Fig. 4). The tensometer was a screw-type testing device that could load a sample in tension or compression, depending on the direction of screw rotation; all loads here were applied in compression. Two types of test were conducted: compression using a broadly distributed load with the sample between the two plates (Fig. 4a), and compression using a concentrated load, with the sample between a point and a plate (Fig. 4b). Point loads were applied using a steel point with a rounded tip with roughly tooth-shaped dimensions (cone height, 14.6 mm; cone angle, 60°; tip radius, 2.6 mm) attached to the dorsal-side steel plate. This point was positioned roughly mid-shell in the middle of a mid-dorsal plate; in particular, at the dorsal midline along the seam between the second and third vertebral scutes (Fig. 4b). The tensometer crosshead was driven using a hand crank at an average speed of 0.15 mm sec^{-1}. Although actual displacement rates during attack by predators are not known, we chose this rate to be as high as possible but still maintain reproducibility; this rate is 18–90 times faster than that used in other studies of turtle bone (Krauss et al., 2009; Rhee et al., 2009; Damiens et al., 2012).

Applied forces were measured using a strain gauge attached to a calibrated force beam. Relative displacements of the loading apparatus were measured using a linear variable differential transformer (LVDT). Voltage data from both the strain gauge and LVDT were collected using an analog-to-digital converter (InstruNet Model 100, GWI, Somerville, MA), attached to a Macintosh computer.

The force-displacement data were used to calculate maximum load, work to failure (area under the force-displacement curve), and relative shell deformation at failure. The point at which the force recording fell below 99% of the maximum load was used as the criterion for failure. Relative shell deformation was defined as the ratio of the dorsoventral deformation at failure to initial shell

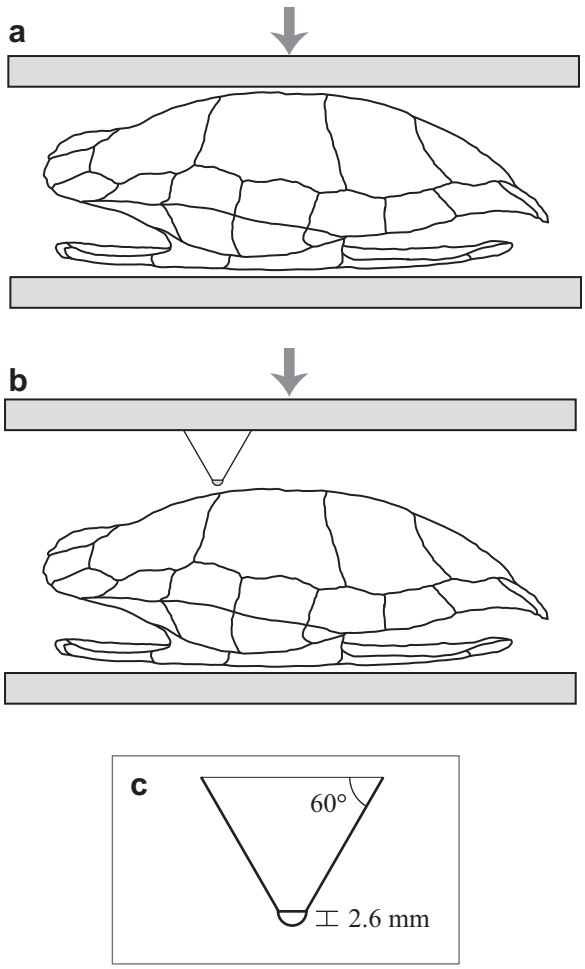

Figure 4. Loading apparatus used in the whole shell loading experiments. (a) Compressive loading; (b) point loading; (c) details of the point loading apparatus. The schematic shows a horizontal orientation for clarity, but in practice the experimental loading rig was oriented such that the plates and turtles were oriented vertically.

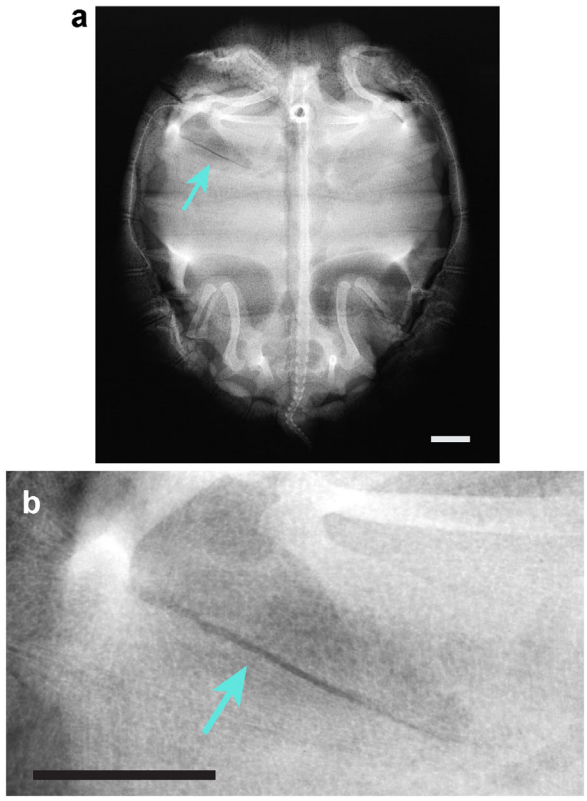

Figure 5. Sample radiograph of *Chrysemys picta* showing location of failure from a broad compression test. (a) Whole shell, dorsoventral view; (b) detail of the only visible crack, ~2 cm in length. The head was removed prior to imaging to enable inspection of the carapace margin. Scale bar, 1 cm.

depth. In practice, the initial depth was measured as the initial distance between the loading plates, and the deformation at failure was the distance traveled by the moving plate. Following the loading tests, the locations and types of fractures were assessed either visually or using dorsoventral radiographs of the specimens (Fig. 5).

Mechanical Properties

After completion of the whole shell loading experiments, bone and suture samples for mechanical testing were excised from the larger specimens. In an attempt to minimize the effects of complex specimen geometry (curvature in particular) and to simplify analyses, we chose plastral tissues rather than carapacial tissues, because the plastron is much flatter than the carapace. Samples were taken from locations remote from the areas of whole shell failure and showed no indication of cracks or deformation, though it is possible that microcracks occurred. Tissue samples were also tested from two additional specimens not included in the whole-shell tests to serve as controls. Bone specimens were taken from the left hypoplastral bone. The suture samples included the hyo-hypoplastral suture for the semi-aquatic taxa and the hypo-xiphiplastral suture for the box turtles. This difference arose because we added box turtles to the study after completing testing with hyo-hyoplastral samples, and therefore had to use a different suture to avoid the box turtle's hinge (Fig. 3).

Tissue samples were excised using a small steel saw blade attached to a rotary dental drill. Tissues were generously bathed in water during cutting to prevent overheating. Samples were cut in the shape of rectangular beams approximately 28 mm long and 3 mm wide, with depth varying depending on the thickness

of the plastron of each individual animal; these bone samples were similar in size to those used by Krauss et al. (2009), who also conducted three-point bending tests of shell bone with and without sutures. Epidermal scutes and periosteal tissues were peeled from exterior and interior surfaces. The edges of the samples were smoothed using fine-grade (400 grit) carborundrum sandpaper to remove any obvious surface defects. Tissue samples were stored in chilled saline solution at 4°C for up to 24 hr. A small amount of calcium leaching may have occurred during storage (Gustafson et al., '96), but this effect is likely to be minor because most samples were tested within 12 hr of preparation.

Mechanical testing was conducted using a symmetrical three-point bending apparatus attached to a tensometer. Specimens were arranged in the bending apparatus with the inner and outer surfaces of the bone in contact with the three posts. Suture samples were loaded with the sutural joint aligned along the mid-span loading beam. The crosshead of the tensometer was hand driven at an average speed of 0.11 mm/sec.

Using force–displacement recordings, four mechanical properties were estimated for each specimen: (i) bending strength (σ_{max}); (ii) maximum ultimate bending strain (ϵ_{max}); (iii) Young's modulus of elasticity; and (iv) energy absorption. Strength refers to the maximum stress (force per unit area) that the specimen can withstand prior to failure, and the ultimate strain indicates its relative displacement. The Young's modulus is a metric of stiffness; the higher the modulus, the stiffer the material.

The stress at any point during bending can be estimated using elastic beam theory. Bending strength is simply the peak stress before failure (Currey, '87; Jaslow, '90). Stresses were calculated from the force–displacement recordings using the formula (Wainwright et al., '76):

$$\sigma = \frac{Mc}{I} \tag{1}$$

where M is the bending moment, I is the second moment of area for the test specimen, and c is one half the mean thickness of the sample. The bending moment, M, was calculated as

$$M = Fd \tag{2}$$

where F represents the applied force, and d is one half the span length of the three-point bending apparatus (i.e., the distance between the loading posts). The second moment of area for a rectangular beam (with respect to the central axis) is

$$I = \frac{wh^3}{12} \tag{3}$$

where w is the sample width and h is the sample height. Because turtle shell bone resembles a sandwich structure, with a cancellous diplöe, this formula should overestimate the true value of I. However, this overestimate provides conservative estimates of stress and strain (see Eqs. 1 and 4). Burstein et al. ('72) have shown that calculating bending strength using the above formula overestimates the true stress when specimens exhibit plastic deformation. However, Currey ('87) and Jaslow ('90) point out that when comparisons are made between similarly sized specimens and the comparisons are relative, bending strength as estimated here can be considered a normalized measure of the bending moment that caused failure. Furthermore, three recent studies of turtle bone (Krauss et al., 2009; Rhee et al., 2009; Damiens et al., 2012) used the same approach, enabling quantitative comparison.

Maximum ultimate bending strains were estimated using the strength-of-materials approach (Hubbard, '71). The strain in the face of a bent rectangular beam can be estimated as:

$$\epsilon = \frac{Mh}{2EI} \tag{4}$$

where E is the modulus of elasticity (Young's modulus). Hubbard ('71) showed that strain values estimated using the strength-of-materials approach for samples of human cranial bone generally agreed well with values measured using strain gauges.

Young's modulus was estimated by calculating the slope of the linearly elastic region of the stress–strain curve. Energy absorption was calculated from the area under the stress–strain curve for each specimen. Energy absorption estimated in this manner is equivalent to work per unit volume.

Following completion of testing, the bone tissue samples were oven-dried (60°C, 4 days) and then ashed (500°C, 3 hr) to determine the ratio of organic-to-mineral content. Samples that included sutures were not included. Mineral content was defined as the percent ash dry weight.

Not all animals used in the study of whole shell behavior could be used for tissue property testing because of restrictions on the minimum size of tissue samples imposed by the loading apparatus. The bulk of the samples used consisted of tissues derived from *T. scripta* individuals. None of the *M. terrapin* specimens were large enough, or well ossified enough, to provide appropriate samples. The mechanical properties for bone were based on a sample of 24 tissue sections from 17 animals. Estimates of suture properties were based on 21 measurements from 16 animals. The small samples sizes for *Chrysemys* (2 bone, 2 suture) and *Terrapene* (4 bone, 2 suture) preclude formal ANOVA's, but we conducted Kruskal–Wallis tests for each variable of interest to determine if there was evidence that the distributions differed among the species. In all cases the test failed to reject the null hypothesis of identical distributions. We therefore grouped the species together for subsequent analyses.

After grouping the samples across species, we excluded one *Trachemys* bone specimen that was a clear outlier. We tested for

normality of each variable for bone and suture samples separately using Shapiro–Wilk tests in combination with quantile–quantile plots. For most variables the Shapiro–Wilk test failed to reject the null hypothesis of normality at $P < 0.05$, except for the modulus of elasticity in the bone samples and ultimate bending strain in the suture samples. We tested for differences in the location parameters for bone versus suture samples using both *t*-tests and non-parameteric Mann–Whitney *U*-tests. *T*-tests are generally robust to modest deviations from normality (Sawilowsky and Blair, '92), and the Mann–Whitney test makes no normality assumptions. Both tests lead to identical conclusions—that the distributions of all of the variables except energy absorption differed between bone and suture.

RESULTS

Structural Properties

Under compressive loading there were two qualitative categories of shell failure. The shells of some specimens failed with an audible cracking sound and a rapid and dramatic decrease of the measured forces. Other specimens failed in a less dramatic manner with little or no audible indication of failure. Specimens failing under this second mode typically reached a force plateau, which slowly dropped as the specimen was deformed further.

Typical force-deformation recordings for compressive and point loadings of whole shells are illustrated in Figure 6a. Maximum force resistance is positively correlated with body size (Fig. 7a and b), but small sample size and a restricted range of body sizes for *Chrysemys*, *Malacelmys*, and *Terrapene* specimens preclude quantitative analysis of potential differences between species. At a given size, the maximal compressive loads that can be resisted were significantly greater than the maximal point loads, but this is not accounted for by differences in the area over which the forces are applied. It is difficult to accurately estimate the stresses borne by the shells in either situation due to the complicated geometry of the shell and the dynamically changing area (which we were not able to measure) over which the forces are applied, but point loading most likely resulted in higher local stress concentrations due to the small area of the point tip.

An alternative metric for comparing responses to compressive and point loads is work to failure. Work to failure, calculated from the force–displacement curves, is a measure of the amount of energy required to induce shell failure. For a given plastron size, the total amount of work required to cause shell failure is similar under compressive and point loads (Fig. 8a).

A third metric for assessing the structural performance of the shell is to examine the maximal fractional deformations of shells, defined as the ratio of displacement depth at failure to original depth. A scatter plot of fractional deformation versus plastron length (Fig. 9) indicates that small animals were able to withstand relatively larger deformations.

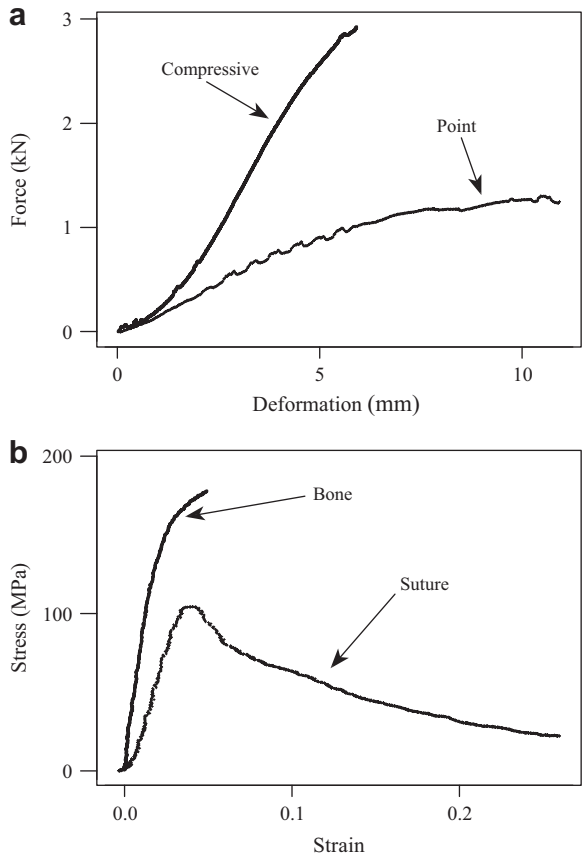

Figure 6. Typical force–displacement and stress–strain traces. (a) Force–displacement trace, whole shells subjected to compressive and point loadings; (b) stress–strain trace for bone and suture tissue samples.

Types and Locations of Shell Failure

When subjected to point loads, most of the *T. scripta* specimens failed at or near the area at which the loads were applied. Failure was indicated by local fracture of the bony tissues immediately surrounding the area of force application. Under compressive loading there were qualitative and quantitative differences between large and small specimens. In large individuals, failure was usually indicated by an immediate decrease in measured load accompanied by audible and dramatic cracking sounds. Shell fractures were visually obvious. Shell failure in smaller individuals was not as dramatic. Force recordings on smaller animals indicated a rise to a maximum load followed by a slowly falling plateau as the shell was deformed further. Small popping sounds were often audible, but there was no indication of a single, catastropic moment of failure. Fracture lines, when recognizable at all, could only be indentified with the use of radiographs.

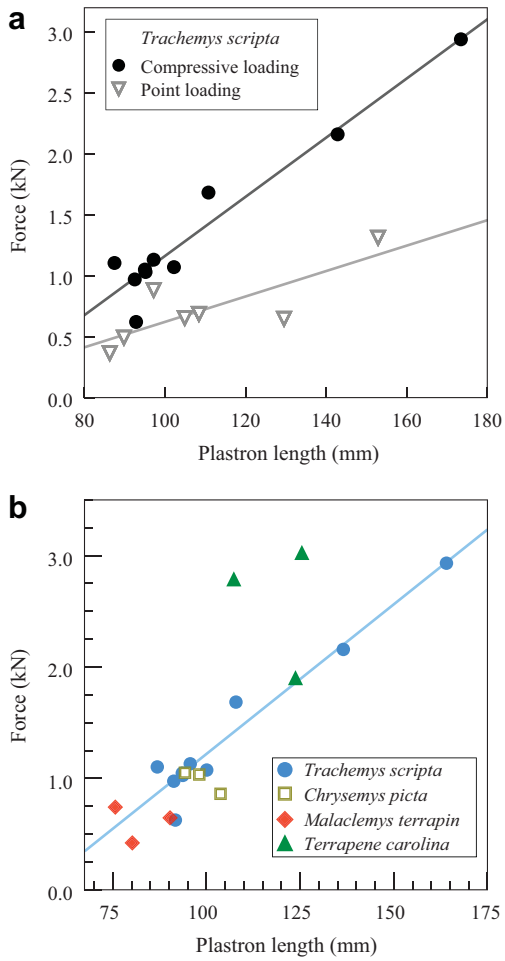

Figure 7. Whole shell, load at failure. (a) Point versus compressive loading, *Trachemys scripta*. The linear regression equations for compressive and point loading are, respectively, $y = -1.27 + 0.024x$, $r^2 = 0.94$, $P < 0.0001$; $y = -0.50 + 0.011x$, $r^2 = 0.71$, $P < 0.001$. (b) Compressive loading, all species. The linear regression equation for *T. scripta* is $y = -1.48 + 0.027x$, $r^2 = 0.93$, $P < 0.0001$.

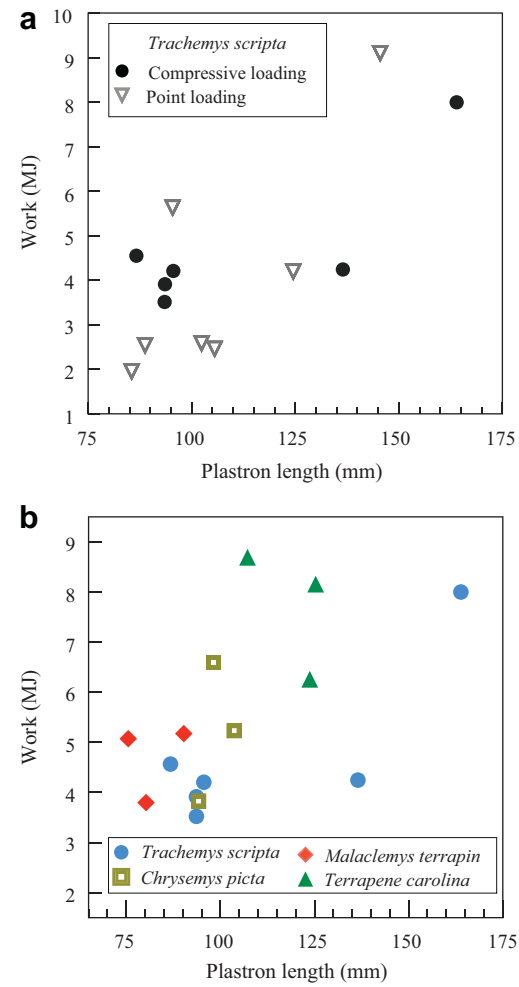

Figure 8. Whole shell, work to failure. (a) Point versus compressive loading, *Trachemys scripta*; (b) compressive loading, all species.

Compressive loading failures in the low-domed taxa (*Trachemys*, *Chrysemys*, *Malaclemys*) were primarily indicated by medio-laterally oriented cracks in the carapace, typically restricted to either the left or right side (Fig. 5). A large proportion of the fractures ran along sulci, which are small depressions in the bony tissue that mark the boundaries between epidermal scutes (Table 1). The sulci are located within the bony plates, which results from the pattern that epidermal scutes do not line up directly over the bony plates (e.g., Claude et al., 2003). Two of the three box turtle specimens failed in a manner dramatically different from the semi-aquatic taxa. These specimens experienced catastrophic cracks in the bridge region joining carapace and plastron. These fractures ran in an anterior–posterior direction, and force records suggest that right and left sides failed almost simultaneously. The shell of the third specimen failed on the left portion of the carapace, rather than along the bridge region.

Mechanical Properties

The means and standard deviations (plus medians and ranges) for each of the mechanical properties measured, pooled across species, are shown in Table 2 and typical stress–strain curves for bone and suture specimens are illustrated in Figure 6b. The mean values of the mechanical properties for suture and bone samples are significantly different for all parameters except energy absorption.

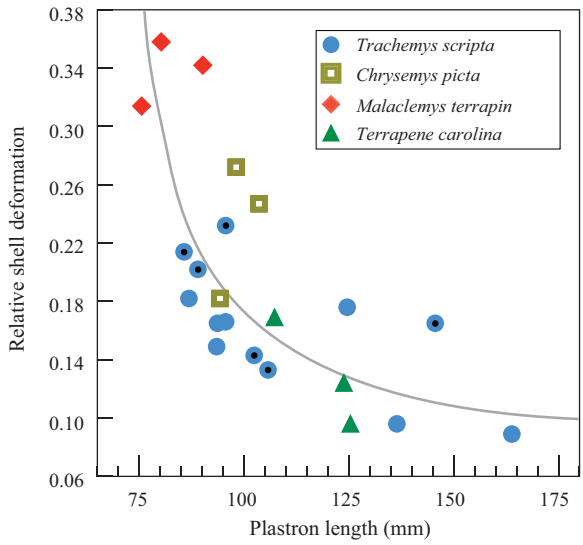

Figure 9. Whole shell, relative deformation. Relative shell deformation is the ratio of the deformation at failure to initial carapace depth. Values from point load tests are indicated with black dots. The curve represents a reciprocal fit with equation $1/y = 15.90 + 1001.5/x$, $r^2 = 0.60$, $P < 0.0001$.

These data suggest that turtle shell sutures (bending strength ~94 MPa) are about two-thirds as strong as the surrounding bone (bending strength ~150 MPa). Despite having lower bending strengths than bone, suture samples absorbed similar amounts of energy (~5.6–6.0 MJ m^{-3}, $P = 0.61$) due to greater ultimate strain values.

The elastic moduli of bone samples ranged from 1.9 to 12.2 GPa (median = 4.7 GPa), whereas the estimates for the suture samples were generally lower, ranging from 0.8 to 5.0 GPa (median = 3.3 GPa).

Mineral content of bone tissues varied between 63% and 78%, with a median value of 68% (dry weight). The largest value represents a sample from a box turtle specimen. Mineral content was negatively correlated with maximum ultimate bending strain ($r = -0.45$, $P = 0.033$; Fig. 10a), and was positively correlated with elastic modulus ($r = 0.40$, $P = 0.058$; Fig. 10b).

DISCUSSION

Whole Shell Structural Properties

We conducted a simple set of loading experiments using whole turtles to provide a baseline understanding of the structural properties of the shell. The degree to which these experiments correspond to natural loading regimes depends upon how turtles are actually mechanically stressed in the wild. Real-world forces may be similar to experimental loads in the way forces are applied (i.e., as compressive or point loads), but real-world forces likely act over much shorter time scales and are applied with more complex geometrical patterns. Because observations of predatory attacks on turtles have been mostly anecdotal, this study took a first-order approach to simulating compressive loading regimes, with the goal of providing experimental data on shell structural and bone tissue characteristics.

Despite the fact that the loadings imposed during our whole-shell tests may not faithfully reproduce natural loads, these

Table 1. Whole shell, locations of failure in compressive loading.

Species and ID	Side	Element
C. picta 1	Both	Costal 2
C. picta 2	L	Costal 2
C. picta 3	R	Costal 4, sulcus between pleurals 2 and 3
T. carolina 1	Both	Bridge/plastron region, crack runs anterior–posterior
T. carolina 1	R	Suture between costals 2 and 3
T. carolina 2	Both	Bridge/plastron region, crack runs anterior–posterior
T. scripta 1	L	Costal 3 and suture between costals 3 and 4
T. scripta 2	L	Costal 2, sulcus between pleurals 1 and 2
T. scripta 3	R	Costal 2, sulcus between pleurals 1 and 2
T. scripta 4	R	Costal 4, sulcus between pleurals 2 and 3
T. scripta 5	L	Suture between nuchal bone and costal 1
T. scripta 6	R	Costal 4, sulcus between pleurals 2 and 3
T. scripta 7	R	Posteriolateral crack crossing costals 4,5 and 6
T. scripta 8	R	Posteriolateral crack crossing costals 4 and 5

All cracks were mediolaterally oriented, except where indicated. Species are *Chrysemys picta*, *Terrapene carolina*, and *Trachemys scripta*.

Table 2. Mechanical properties of turtle shell bone and sutures, pooled across species.

Tissue parameter	Bone ($n = 24$)	Suture ($n = 21$)	Bone and suture different at $P < 0.05$
Modulus of elasticity (GPa)	5.0 ± 2.4	3.0 ± 1.0	Yes
	1.9–12.2 (4.7)	0.8–5.0 (3.3)	
Bending strength (MPa)	151.3 ± 42.4	93.9 ± 33.0	Yes
	74–228 (149)	34–160 (97)	
Maximum ultimate bending strain	0.059 ± 0.018	0.088 ± 0.030	Yes
	0.025–0.11 (0.06)	0.05–0.18 (0.08)	
Energy absorption (MJ m^{-3})	6.0 ± 3.6	5.6 ± 1.5	No
	1.9–18.4 (5.1)	2.7–8.8 (5.6)	
Mineral content	0.68 ± 0.03	–	–
	0.63–0.78 (0.68)		

The first line in each cell gives the mean and standard deviations, the second line gives the range and median for each value.

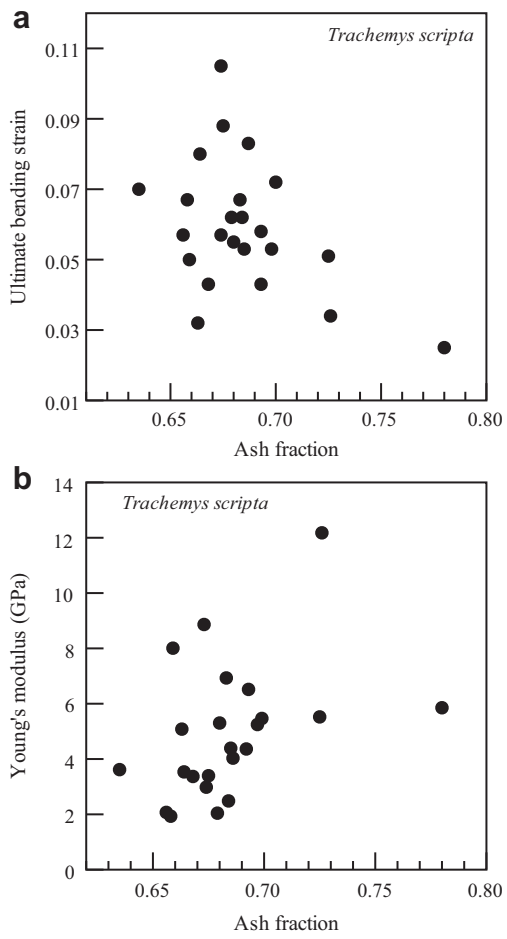

Figure 10. Tissue properties, relationships with mineral content. (a) Relationship between maximum ultimate bending strain and ash fraction; (b) relationship between Young's modulus and ash fraction.

experiments nonetheless provide useful information about shell failure. The compressive loading experiments suggest that the sulci that mark the borders between epidermal scutes are zones of weakness. The sulci are somewhat thinner than the surrounding bone and may be more susceptible to accumulating microdamage. Shell geometry and the macroscopic appearance of fracture surfaces suggest that dorsally applied compressive loads result in the failure of lateral shell elements (costal and peripheral bones). In multiple finite element modeling studies, Stayton and coworkers have found that the highest stresses should occur in the bridge region of the shell (Stayton, 2009; Rivera and Stayton, 2011; Vega and Stayton, 2011). In contrast, only 2 (of 14) of our whole-shell compression tests resulted in failure at the bridge region. These two specimens were box turtles, whose bridges between the plastron and carapace are largely composed of ligament rather than bone (Stayton, 2011) and clearly represent a zone of weakness in the shell. The differences between our experimental results and those suggested by stress distributions in finite element models may be explained by differences in the details of loading between the experiments and models, or by the differences in shell shape between species in our study and those examined by Stayton and coworkers (*Chrysemys*, *Glyptemys*, and *Pseudemys* spp.). These results also suggest that current finite element models of turtles require further refinements to better reflect variations in material properties and the structural interactions of the components of the shell system.

Few of the shell failures appear to have begun at the sutural joints. We found that sutures, despite being relatively weaker in bending, deform more and can absorb similar amounts of energy relative to the surrounding bone. Such properties may explain why these interfaces between bony elements were not the sites of failure in most of the whole-shell tests. Krauss et al. (2009) examined turtle sutures on a finer scale and showed that the collagen fiber orientation within the suture is arranged such that the fibers are loaded in tension when the shell is loaded in compression. They also found a gradient in mineral concentration

that decreases from the bone toward the suture, which itself is devoid of minerals. Bone with lower mineral content is less stiff and more flexible, consistent with our comparative findings between plastron bone with and without sutures. Lastly, their study showed that, although a suture is flexible at small loads, it becomes more rigid with larger loads (likely due to viscoelastic effects), which may help explain how forces could be transmitted effectively across sutures during shell compression. Overall, the results from our tests of isolated suture samples are consistent with previous understanding of suture properties and help provide some explanation for how shells withstand forces, but the complexity of the suture morphology and loading suggest that more detailed modeling is necessary for greater insight into shell behavior.

The whole-shell loading experiments also highlight the fact that, while larger individuals can bear relatively larger forces, smaller individuals were able to withstand relatively greater dorsoventral deformations before the shell failed. This is likely attributable to the fact that younger individuals are less fully ossified, and still retain fontanelles of dense connective tissue near the margins of the shell between the costal and peripheral plates. This dense connective tissue is more extensible than the surrounding bone and thus the structure as a whole is able to bear greater deformations. Furthermore, the smaller individuals had absolutely thinner bone, which should also permit greater structural deformation under a given load.

For a given plastron size, the total amount of work required to cause shell failure is similar under both compressive and point loads (Fig. 8a). Failure under compressive loading was often dramatic and marked by a rapid and large decrease in measured force. Unexpectedly, failure under point loads was more gradual, and shells continued to bear significant forces even after "failing" according to the defined criterion (99% maximum load). A different failure criterion, such as a failure cut-off point of 75% of maximum load, would decrease the assessment of work to failure for the point loading experiments while leaving the values for the compressive loadings relatively unchanged. An additional explanation for this gradual failure behavior under point loading may be that a small hole was created in the shell, which then became progressively larger as the load increased, but our tests were not able to distinguish such details.

Bone Mechanical Properties

We used three-point bending tests and simple beam theory to calculate stress and strain in rectangular bone sample from the relatively flat plastron. Turtle shell bone is a type of "sandwich bone", consisting of inner and outer layers of compact bone that surround a cancellous, spongy tissue (diplöe). Indentation testing of the separate layers has shown that the outer layers are much more stiff and less extensible than the inner layer, with Young's modulus values ranging from 0.5 to 22 GPa (Balani et al., 2011). Our calculated values of Young's modulus (2–12 GPa) are consistent with the overall modulus of the shell (~5 GPa) as modeled by Balani and coworkers using individual layer values. Our values are smaller than those reported from other three-point bending tests (18–25 GPa; Rhee et al., 2009), but this may reflect differences in experimental protocol (such as loading rate) or the location from which the bone samples were chosen (plastron vs. carapace).

These combined analyses of the dermal components of the turtle shell help to build a framework for understanding how the tissues that make up the shell are suited to their role in providing protection. Both bone and sutures absorb relatively large amounts of energy per unit volume before fracturing. Sutures are weaker than the surrounding bone, but are able to absorb similar amounts of energy due to their greater extensibility. Reptiles in general may have particularly high yield strains. Blob and Biewener ('99) found that limb bones of alligator and iguana have higher yield strains than those of birds or mammals, and Currey ('87) found that the limb bones of Galapagos tortoises (*Geochelone elephantopus*) had some of the highest values for ultimate strain and energy absorption of any of the amniote bones he tested except antler.

CONCLUSIONS

The results of this study provide baseline data as to how effective the turtle's unique skeletal structure is in resisting mechanical loads. Whole-shell structural studies provide estimates of the forces that shells can resist under both compressive and point loads as well as the total work required to cause significant damage. The results of the structural experiments are also suggestive of further hypotheses to be considered in investigations of how shell morphology affects stress distributions and mode of failure. In particular, future studies should investigate the origin of why failure occurs in regions away from the bridge elements, which seem to be areas of weakness.

It is hoped that this initial set of studies into the structural and mechanical properties of turtle shells will provide a basis for further research. Additional ontogenetic studies of bone/shell properties and organization will be particularly valuable for assessing the relationships between the amount of overall shell ossification, the mineral fraction of ossified tissues, and the structural and mechanical properties of shells. With respect to structural properties of the shell, more realistic and more complex loading regimes will provide valuable insight into the ability of the shell to withstand attacks from predators. Detailed field experiments and descriptions of the natural history of turtles (e.g., Emmons, '89) are needed to provide such accurate information about turtle-predator interactions. Lastly, biomechanical studies of shell properties should be coupled with studies of ecologically relevant areas such as the hydrodynamic effects of shells (as in Rivera and Stayton, 2011), costs of transport, or reproductive capacity. A combination of such approaches will be critical for assessing the potential fitness benefits associated with variations in shell morphology.

ACKNOWLEDGMENTS

This work was conducted as part of the doctoral research of one of the authors (PMM). We thank Michael LaBarbera, Rick Blob, Nora Espinoza, Tristan Stayton, Michael Madigan, and two anonymous reviewers for their critical comments and suggestions on the manuscript.

LITERATURE CITED

Balani K, Patel RR, Keshri AK, Lahiri D, Agarwal A. 2011. Multi-scale hierarchy of *Chelydra serpentina*: microstructure and mechanical properties of turtle shell. J Mech Behav Biomed Mater 4:1440–1451.

Blob RW, Biewener AA. 1999. *In vivo* locomotor strain in the hindlimb bones of *Alligator mississippiensis* and *Iguana iguana*: implications for the evolution of limb bone safety factor and non-sprawling limb posture. J Exp Biol 202:1023–1046.

Borchers RE, Gibson LJ, Burchardt H, Hayes WC. 1995. Effects of selected thermal variables on the mechanical properties of trabecular bone. Biomaterials 16:545–551.

Bramble DM. 1974. Emydid shell kinesis: biomechanics and evolution. Copeia 1974:707–727.

Bramble DM, Hutchison JH, Legler JM. 1984. Kinosternid shell kinesis: structure, function and evolution. Copeia 84:456–475.

Branch WR, Els SF. 1990. Predation on the angulate tortoise *Chersina angulata* by the kelp gull *Larus dominicanus* on Dassen Island, Western Cape. S Afr J Zool 25:235–237.

Burstein AH, Currey JD, Frankel VH, Reilly DT. 1972. The ultimate properties of bone tissue: the effects of yielding. J Biomech 5:35–44.

Claude J, Paradis E, Tong H, Auffray J-C. 2003. A geometric morphometric assessment of the effects of environment and cladogenesis on the evolution of the turtle shell. Biol J Linn Soc 79:485–501.

Congdon JD, Gibbons JW. 1990. The evolution of turtle life histories. In: Gibbons JW, editor. Life history and ecology of the slider turtle. Washington, DC: Smithsonian Institution Press. p 45–54.

Currey JD. 1987. The evolution of the mechanical properties of amniote bone. J Biomech 20:1035–1044.

Damiens R, Rhee H, Hwang Y, et al. 2012. Compressive behavior of a turtle's shell: experiment, modeling, and simulation. J Mech Behav Biomed Mater 6:106–112.

Emmons LH. 1989. Jaguar predation on chelonians. J Herpetol 23: 311–314.

Erickson GM, Lappin AK, Vliet KA. 2003. The ontogeny of bite-force performance in American alligator (*Alligator mississippiensis*). J Zool Lond 260:317–327.

Ernst CH, Lovich JE, Barbour RW. 1994. Turtles of the United States and Canada. Washington, DC: Smithsonian Institution Press.

Franklin CJ. 2007. Turtles: an extraordinary natural history 245 million years in the making. Minneapolis: Voyageur Press.

Gaffney ES, Meylan PA. 1988. A phylogeny of turtles. In: Benton MJ, editor. The phylogeny and classification of the tetrapods, Vol. 1: amphibians, reptiles, birds. Oxford: Clarendon Press. p 157–219.

Gustafson MB, Martin RB, Gibson V, et al. 1996. Calcium buffering is required to maintain bone stiffness in saline solution. J Biomech 29:1191–1194.

Heithaus HR, Wirsing AJ, Thomson JA, Burkholder DA. 2008. A review of lethal and non-lethal effects of predators on adult marine turtles. J Exp Mar Biol Ecol 356:43–51.

Hubbard RP. 1971. Flexure of layered cranial bone. J Biomech 4:251–263.

Iverson JB. 1991. Life history and demography of the yellow mud turtle, *Kinosternon flavescens*. Herpetologica 47:373–395.

Jackson DC. 1997. Lactate accumulation in the shell of the turtle *Chrysemys picta bellii* during anoxia at 3°C and 10°C. J Exp Biol 200:2295–2300.

Jaslow CR. 1990. Mechanical properties of cranial sutures. J Biomech 23:313–321.

Krauss S, Monsonego-Ornan E, Zelzer E, Fratzl P, Shahar R. 2009. Biological materials: mechanical function of a complex three-dimensional suture joining the bony elements in the shell of the red-eared slider turtle. Adv Mater 21:407–412.

Landberg T, Mailhot J, Brainerd EL. 2003. Lung ventilation during treadmill locomotion in a terrestrial turtle, *Terrapene carolina*. J Exp Biol 206:3391–3404.

Moreno J, Forriol F. 2002. Effects of preservation on the mechanical strength and chemical composition of cortical bone: an experimental study in sheep femora. Biomaterials 23:2615–2619.

Pelker RR, Friedlaender GE, Markham TC, Panjabi MM, Moen CJ. 1983. Effects of freezing and freeze-drying on the biomechanical properties of rat bone. J Orthop Res 1:405–411.

Ramaekers JGM. 1979. The rheological behavior of skeletal material originating from several classes of vertebrates. Neth J Zool 29: 166–176.

Rhee H, Horstemeyer MF, Hwang Y, et al. 2009. A study on the structure and mechanical behavior of the *Terrapene carolina* carapace: a pathway to design bio-inspired synthetic composites. Mater Sci Eng C 29:2333–2339.

Richmond ND. 1964. The mechanical functions of the testudinate plastron. Am Midl Nat 72:50–56.

Rieppel O. 1993. Studies on skeleton formation in reptiles: patterns of ossification in the skeleton of Chelydra serpentina (Reptilia, Testudines). J Zool Lond 231:487–509.

Rivera G, Stayton CT. 2011. Finite element modeling of shell shape in the freshwater turtle *Pseudemys concinna* reveals a trade-off between mechanical strength and hydrodynamic efficiency. J Morphol 272:1192–1203.

Rosenberg ME. 1986. Carapace and plastron sensitivity to touch and vibration in the tortoise (*Testudo hermanni* and *T. graeca*). J Zool Lond 208:443–455.

Sawilowsky S, Blair RC. 1992. A more realistic look at the robustness and type II error properties of the t test to departures from population normality. Psychol Bull 111:353–360.

Seidel ME, Atkins MD. 1989. Variation in turtle myoglobins (Subfamily Emydinae: Testudines) examined by isoelectric focusing. Comp Biochem Physiol B 94:569–574.

Stayton CT. 2009. Application of thin-plate spline transformations to finite element models, or, how to turn a bog turtle into a spotted turtle to analyze both. Evolution 63:1348–1355.

Stayton CT. 2011. Biomechanics on the half shell: functional performance influences patterns of morphological variation in the emydid turtle carapace. Zoology 114:213–223.

Shipman PA, Edds DR, Blex D. 1994. *Macroclemys temminckii* (alligator snapping turtle) and *Chelydra serpentina* (common snapping turtle). Agonistic behavior. Herp Rev 25:24–25.

Vega C, Stayton CT. 2011. Dimorphism in shell shape and strength in two species of emydid turtle. Herpetologica 67: 397–405.

Wainwright SA, Biggs WD, Currey JD, Gosline JM. 1976. Mechanical design in organisms. New York: John Wiley and Sons.

Walley HD. 1993. *Chelydra serpentina* (Snapping Turtle). Predation. Herpetol Rev 24:148–149.

Zangerl R. 1969. The turtle shell. In: Gans C, Bellairs AdA, Parsons TS, editors. Biology of the reptilia, Vol. 1. New York: Academic Press. p 311–339.

Zhang W, Wu C, Zhang C, Chen Z. 2012a. Microstructure and mechanical property of turtle shell. Theor Appl Mech Lett 2: 014009.

Zhang W, Wu C, Zhang C, Chen Z. 2012b. Numerical study of the mechanical response of turtle shell. J Bionic Eng 9:330–335.